

Uncertainty in eddy covariance measurements and its application to physiological models

D. Y. HOLLINGER^{1,2} and A. D. RICHARDSON³

¹ USDA Forest Service NE Research Station, 271 Mast Road, Durham, NH 03824, USA

² Corresponding author (dhollinger@fs.fed.us)

³ Complex Systems Research Center, University of New Hampshire, Durham, NH 03824, USA

Received September 9, 2004; accepted January 15, 2005; published online May 2, 2005

Summary Flux data are noisy, and this uncertainty is largely due to random measurement error. Knowledge of uncertainty is essential for the statistical evaluation of modeled and measured fluxes, for comparison of parameters derived by fitting models to measured fluxes and in formal data-assimilation efforts. We used the difference between simultaneous measurements from two towers located less than 1 km apart to quantify the distributional characteristics of the measurement error in fluxes of carbon dioxide (CO₂) and sensible and latent heat (*H* and *LE*, respectively). Flux measurement error more closely follows a double exponential than a normal distribution. The CO₂ flux uncertainty is negatively correlated with mean wind speed, whereas uncertainty in *H* and *LE* is positively correlated with net radiation flux.

Measurements from a single tower made 24 h apart under similar environmental conditions can also be used to characterize flux uncertainty. Uncertainty calculated by this method is somewhat higher than that derived from the two-tower approach. We demonstrate the use of flux uncertainty in maximum likelihood parameter estimates for simple physiological models of daytime net carbon exchange. We show that inferred model parameters are highly correlated, and that hypothesis testing is therefore possible only when the joint distribution of the model parameters is taken into account.

Keywords: AmeriFlux, forest CO₂ exchange, Howland, Monte Carlo.

Introduction

Carbon dioxide (CO₂) and other flux data now accumulating from sites around the world (Baldocchi et al. 2003) are valuable resources for assessing models of ecosystem physiology. For such comparisons to be meaningful, however, the uncertainty in both the model and the flux data used for validation must be specified. With knowledge of measurement data and model uncertainty, the model may be accepted or rejected with some level of confidence.

Alternatively, sometimes it is desirable to use flux data to determine parameter values of a specified model. Maximum likelihood methods (e.g., Bevington and Robinson 1992, Press

et al. 1993) can provide unbiased estimates of model parameters from experimental data, and several authors have applied these or related approaches to eddy flux data (e.g., Schulz et al. 2001, van Wijk and Bouten 2002, Hollinger et al. 2004). A problem with this approach for many simple models, including those of surface–atmosphere fluxes, is equifinality in the parameter sets (Franks et al. 1997, Schulz et al. 2001). Equifinality means that instead of a single set of model parameters being clearly optimal, there may be many sets of parameter values that all fit the flux data more or less equally well. The magnitude of this problem generally increases as model complexity is increased (Franks et al. 1997). However, with knowledge of the uncertainty inherent in flux measurements, it is possible not only to properly describe the confidence intervals of model parameter estimates, but also to obtain more precise parameter estimates.

A broader but related question is that of choosing the correct model. Understanding the magnitude and causes of uncertainty in flux data can help constrain the universe of potential models that account for the data. Schulz et al. (2001), for example, found that the information content of several weeks of eddy flux data was insufficient to support the calibration of many components of a biochemically based model of carbon exchange. Jarvis et al. (2004) drew attention to the need for the complexity of a flux model to be commensurate with the information content of the calibration data. Making full use of the information content of flux data, including the uncertainty, allows for the assessment and comparison of various physiological models.

Measurement error

Since measurement error is a random variable, the size of the error depends on chance; ideally, we would know the complete probability distribution of the error, or a density function (and the associated parameters) that approximates the distribution of the error. At a minimum, we need to know the mean and an estimate of the dispersion, such as the standard deviation, of the measurement error. It may also be useful to know whether the measurement error varies in relation to other factors (e.g., time of day, day of year, wind speed, net radiation, or magnitude of the measured flux).

Uncertainty can be quantified in several ways, and we will use the most common, the standard deviation (σ) of the underlying error, where $\pm 1\sigma$ encompasses 68.3% of the probability density function for a Gaussian distribution. Often error analyses consider random error separately from systematic error or bias (Taylor 1997) because the former uncertainties can be revealed by statistical analysis whereas systematic errors cannot. Systematic errors can often be removed by calibration, whereas this is not possible with random error. Flux measurements are often affected by systematic errors including lack of energy balance closure and incomplete measurement of nocturnal CO₂ exchange. The causes of these systematic errors and potential remedies are an active area of research (e.g., Businger 1986, Goulden et al. 1996, Moncrieff et al. 1996, Mahrt 1998, Twine et al. 2000, Massman and Lee 2002, Morgenstern et al. 2004).

Flux measurements are unusual in that the actions of a population of flux absorbers and emitters (leaves, soil, stems, logs, etc.) are integrated and transmitted to the measurement system via the stochastic and intermittent process of turbulent transport (eddies). Random measurement errors in flux data thus result from several different sources. These include errors associated with the flux measurement system (gas analyzer, sonic anemometer, data acquisition system, flux calculations), errors associated with turbulent transport, and statistical errors relating to the location and activity of the sites of flux exchange ("footprint heterogeneity") (Moncrieff et al. 1996).

Uncertainty in turbulent transport has been discussed as the primary source of flux uncertainty by several authors (e.g., Lenschow et al. 1994, Mann and Lenschow 1994, Finkelstein and Sims 2001). Traditionally (Mahrt 1998), the relative random error in flux measurements (RE) has been estimated as the variance computed from the individual high-frequency data points in a standard (e.g., 30-min) record as:

$$RE = \left(\frac{2 \text{var}(\text{flux})\tau_f}{T} \right)^{0.5} \quad (1)$$

where τ_f is the integral timescale (frequency peak of cospectrum), and T is the averaging time. Since both the variance and τ_f must be estimated from the data, Equation 1 provides only an estimate of the error. Finkelstein and Sims' (2001) method for determining the variance of a covariance includes necessary auto- and cross-covariance terms, but still relies on estimates of the cospectral shape and τ_f .

The uncertainty in a measurement can also be characterized by making multiple measurements of a process and then using the variability of these measurements to estimate the standard deviation of the uncertainty. In the case of flux data, this involves examining the variance of multiple (e.g., 30-min) records. However, as Mahrt (1998) points out, for this approach to work, the process must be stationary, meaning that all of its statistical parameters are independent of time. Over the course of a day or a season, this is generally not the case with flux data, which are strongly affected by solar forcing and temperature. It is this variation, in fact, that we are often trying to capture with a physiologically based model. Binning the data by a

covariate such as solar radiation can reduce the problem, but other confounding factors such as precipitation and temperature may result in additional variability beyond that due to measurement uncertainty alone. Additionally, flux exchange may not be stationary because phenological or physiological changes occur, meaning that the exchange characteristics of the surface itself (for example, CO₂ uptake per unit incident photosynthetically active photon flux density, PPF) vary over time (e.g., Hollinger et al. 2004).

A pair of independent flux measurements made repeatedly under identical conditions (ideally, this would mean simultaneously), provides a solution to many of the problems described above. In this case, if the flux process has true value \bar{x} , we will actually measure the following pair X_1, X_2 :

$$X_1 = \bar{x} + \delta q_1 \quad (2A)$$

$$X_2 = \bar{x} + \delta q_2 \quad (2B)$$

Here the measurement uncertainty (δq_i) is a realization of a random variable with mean 0 and standard deviation $\sigma(\delta q)$. To characterize the uncertainty in our measurements, we want to determine the value of $\sigma(\delta q)$. Because the expected value of $(X_1 - X_2)$ is 0, the variance of $(X_1 - X_2)$ equals the variance of $(\delta q_1 - \delta q_2)$, which is given by:

$$\sigma^2(\delta q_1 - \delta q_2) = \sigma^2(\delta q_1) + \sigma^2(\delta q_2) + 2 \text{cov}(\delta q_1, \delta q_2) \quad (3)$$

Since δq_1 and δq_2 are independent and identically distributed, the right hand of Equation 3 simplifies to $2\sigma^2(\delta q)$. Thus:

$$\sigma(\delta q) = \frac{1}{\sqrt{2}} \sigma(X_1 - X_2) \quad (4)$$

Therefore, by repeating the paired measurements X_1 and X_2 , we can estimate $\sigma(\delta q)$ by calculating the standard deviation of the difference $(X_1 - X_2)$.

Here we characterize the random error in surface-atmosphere flux measurements, with a unique two-tower system located at the Howland AmeriFlux site in Maine, USA (Hollinger et al. 2004). The towers provide simultaneous and independent measurements of surface fluxes and meteorological driving variables that offer a straightforward route to calculating uncertainty. We compare the two-tower results with traditional meteorological methods and then demonstrate that flux uncertainty can also be adequately characterized by selective binning of data and thus does not require paired towers or assumptions about cospectral shapes or integral timescales. We also illustrate how the uncertainty estimates can be employed in maximum likelihood estimates of model parameters using a simple physiologically based model of net CO₂ exchange.

Maximum likelihood (ML) methods approach parameter estimation from a probabilistic basis, considering the probability that a data set (\pm some Δy on each data point) results from a specific set of model parameters (Press et al. 1993). This probability is considered the likelihood of the parameters given the data. The goal then is to find the parameter set that

maximizes the likelihood as defined above. To do this formally requires the knowledge (or choice) of a probability density function (PDF) which describes the measurement error as well as the specification of the model, $y(x)$. The probability of the data set (P) is the product of the probabilities of each data point. If the measurement errors are Gaussian with the same uncertainty (σ) for each of N data points, y :

$$P \propto \prod_i^N e^{\left(-\frac{1}{2}\left(\frac{y_i - y(x_i)}{\sigma}\right)^2\right)} \Delta y \quad (5)$$

For convenience, it is often desirable to maximize the logarithm (or minimize the negative of the logarithm) of the likelihood function above.

In later discussion, we will consider two models for our $y(x)$. The first is a simple “big-leaf” model consisting of the 3-parameter Michaelis-Menten equation that relates daytime net ecosystem exchange (NEE) to incident PPFD, I , as:

$$\text{NEE} = \frac{A_{\max} I}{K_m + I} - R \quad (6)$$

where A_{\max} is a maximum rate of uptake, K_m is the half-saturation constant and R is ecosystem respiration. The second model combines leaf photosynthesis with Norman’s (1980, 1982) simple sun–shade canopy model. For canopies with a spherical leaf angle distribution (leaf angle and azimuth determined from random locations on a spherical surface), the sunlit leaf area index (LAI) is F_{sun} and the shaded LAI is F_{shade} , as follows:

$$F_{\text{sun}} = \left(1 - e^{\frac{-0.5F}{\sin(\theta)}}\right) 2 \sin(\theta) \quad (7)$$

$$F_{\text{shade}} = F - F_{\text{sun}} \quad (8)$$

where F is the total LAI and θ is the solar elevation. The PPFD on the shaded leaves is the sum of scattered direct beam and diffuse PPFD and can be approximated as:

$$I_{\text{shade}} = I_{\text{dir}} e^{(-0.5F^{0.7})} + C \quad (9)$$

where the left half of the equation represents extinction of the diffuse component and C is the scattered component and I_{dir} is the diffuse PPFD on a horizontal plane above the canopy. Norman (1982) expresses the scattered component of the direct beam as:

$$C = k I_{\text{dir}} (1.1 - 0.1F) e^{-\sin(\theta)} \quad (10)$$

where k is a scattering coefficient (equal to two thirds of the difference between 1 and the leaf absorptance), I_{dir} is the horizontal beam PPFD and the other terms account for decreased scattering with depth and increased scattering with low sun angles. The PPFD striking the sunlit leaves can be expressed as:

$$I_{\text{sun}} = \frac{I_{\text{dir}} \cos(a)}{\sin(\theta)} + I_{\text{shade}} \quad (11)$$

where a is the mean leaf–sun angle (Ross 1981) and is equal to 60° for a spherical leaf angle distribution. NEE is then calculated by summing the photosynthesis for leaves of the two light classes and multiplying by the appropriate sunlit and shaded leaf area indexes:

$$\text{NEE} = F_{\text{sun}} \left(\frac{I_{\text{sun}} A_{\text{leaf}}}{I_{\text{sun}} + K_{\text{leaf}}} + R_{\text{leaf}} \right) + F_{\text{shade}} \left(\frac{I_{\text{shade}} A_{\text{leaf}}}{I_{\text{shade}} + K_{\text{leaf}}} + R_{\text{leaf}} \right) + R_{\text{leaf}} F \quad (12)$$

The canopy is composed of identical leaves with photosynthetic parameters (A_{leaf} , K_{leaf} and R_{leaf} , which are the leaf-level equivalents of the A_{\max} , K_m and R parameters previously defined, and absorptance = 0.9). The final term in Equation 12 accounts for the observation that one-half of total ecosystem respiration at Howland is from the soil (Davidson et al. 2005).

Materials and methods

Site description

Flux measurements were made at the Howland Forest AmeriFlux site located about 35 miles north of Bangor, ME ($45^\circ 15' \text{ N}$, $68^\circ 44' \text{ W}$, 60 m a.s.l.) on commercial forestland owned by the International Paper Company. Forest stands are dominated by red spruce (*Picea rubens* Sarg.) and eastern hemlock (*Tsuga canadensis* (L.) Carr.) with lesser quantities of other conifers and hardwoods. Fernandez et al. (1993) and Hollinger et al. (1999) have previously described the climate, soils and vegetation at Howland.

Data were recorded from two research towers separated by about 775 m and instrumented with identical eddy covariance systems. The first flux tower (“main” tower, 45.20407° N , 68.74020° W) was established in 1995 and the second (“west” tower, 45.20912° N , 68.74700° W) in 1998.

Flux measurements

Fluxes were measured at a height of 29 m with systems consisting of model SAT-211/3K 3-axis sonic anemometers (Applied Technologies, Longmont, CO) and model LI-6262 fast response $\text{CO}_2/\text{H}_2\text{O}$ infrared gas analyzers (Li-Cor, Lincoln, NE), with data recorded at 5 Hz. The flux measurement systems and calculations are described in detail in Hollinger et al. (1999, 2004). Deficiencies in the low and high frequency response of the flux systems were corrected by using the Horst/Massman approach of calculating a transfer function based on stability and theoretical spectra (e.g., Horst 1997, 2000, Massman 2000, 2001) to correct for missing low frequency contributions and a ratio of filtered to unfiltered heat fluxes to account for missing high frequency fluctuations. Half-hourly flux values were excluded from further analysis if the wind speed was below 0.5 m s^{-1} , scalar variance was excessively

high or extremely low (Hollinger et al. 1995), rain or snow was falling, half-hour sample periods were incomplete or there was an instrument malfunction. Data from nocturnal periods were excluded when the friction velocity (u_*) was less than a threshold of 0.25 m s^{-1} . The sign convention used is that carbon flux into the ecosystem is defined as negative.

Statistical fitting

To calculate maximum likelihood values, we used the Monte Carlo method with simulated annealing (Metropolis et al. 1953) to minimize the merit function given by the chi-square statistic, χ^2 . If the measurement errors are normally distributed, the logarithm of Equation 5 indicates that the appropriate χ^2 is the weighted sum of the squared differences between measured (y_i) and modeled $y(x_i)$ values, with the square of the measurement error uncertainty (σ) used as the weighting factor (Press et al. 1993):

$$\chi^2 = \sum_i^N \frac{(y_i - y(x_i))^2}{\sigma^2} \quad (13)$$

If σ is identical for all data, this equates to an ordinary least squares minimization. Different merit functions deriving from different ML functions are necessary if measurement errors are not normally distributed. For example, when the measurement errors follow the double exponential distribution, the merit function is (Press et al. 1993):

$$\chi^2 = \sum_i^N \frac{|y_i - y(x_i)|}{\sigma} \quad (14)$$

where $\sigma = \sqrt{2}\beta$ and β is the mean of the absolute deviations of the samples from their mean.

In the simulated annealing procedure, an iterative random walk method is used to determine the optimal set of model parameters, as follows. At each step, j , a new set of model parameters ($p_j^1 \dots p_j^n$) is generated by randomly perturbing the previous set of parameters ($p_{j-1}^1 \dots p_{j-1}^n$) by a small amount. The new set is adopted if $\chi_j^2 < \chi_{j-1}^2$, otherwise the previous set of parameters is retained. To keep the procedure from becoming stuck in local minima, the new set of parameters will also be adopted when $\chi_j^2 > \chi_{j-1}^2$ with probability proportional to:

$$e^{-\frac{(\chi_j^2 - \chi_{j-1}^2)}{k}} \quad (15)$$

where k is an effective temperature. This process is repeated many thousands of times, with the magnitude of k gradually declining, until a predetermined stopping criterion is met.

Traditional method of estimating flux uncertainty

Lenschow et al. (1994) and Mann and Lenschow (1994) developed an estimate for the relative error in an aircraft flux measurement based on two joint-normally distributed variables as:

$$\frac{\sigma_F(L)}{|F|} = \left(\frac{2\tau_f}{L} \right)^{0.5} \left(\frac{1+r_{wc}^2}{r_{wc}^2} \right)^{0.5} (1 - az_*) \quad (16)$$

where L is the length of the flight leg, r_{wc} is the correlation coefficient between the vertical wind velocity w , and scalar c , (we note $r_{wc} = \text{cov}(wc)/(\sigma_w\sigma_c)$) and az_* is the relative height of the aircraft within the boundary layer. For the surface (tower) approximation, L is the sample period (1800 s), for daytime conditions $\tau_f = z/\bar{u}$ where z is the measurement height and \bar{u} is the 30-min mean wind speed, and $az_* = 0$. We did not attempt to evaluate Equation 16 at night when we had little information about the cospectral shape or integral timescale. Where estimates of absolute uncertainty are presented, the results of Equation 16 were multiplied by the absolute value of the measured flux. This equation was evaluated with data from the main tower.

Estimating uncertainty in flux data

The two towers at Howland are separated by sufficient distance that the flux source regions over a half-hour time period do not generally overlap, providing independent but simultaneous measures of heat, water vapor and CO_2 fluxes (H , LE and F_{CO_2}), with mean differences between the two tower fluxes that are close to zero (Hollinger et al. 2004). Assuming that the error from each tower contributes equally to the error in the difference, the uncertainty (expressed as a standard deviation) in the measured flux at one tower can be calculated from Equation 4 with X_1 and X_2 representing simultaneous measurements from the main and west towers, respectively. Because meteorological conditions at the two towers are nearly identical (Hollinger et al. 2004), the flux uncertainty $\sigma(\delta q)$ can then be analyzed in relation to some block of time or measurement conditions (half-hourly mean PPFD, wind, etc.).

Paired observations from one tower to estimate uncertainty

There are few flux sites where two appropriately distanced towers simultaneously measure fluxes from patches of similar vegetation. We therefore developed a method that would enable the estimation of $\sigma(\delta q)$ even when researchers do not have the good fortune of a second tower. In this approach we trade time for space, and use flux measurements made on two successive days at one tower as analogues of the simultaneous two-tower paired measurements described above. A measurement pair was considered valid only if both measurements were made under "equivalent" conditions, defined here as at the same time of day (to minimize diurnal effects) and under nearly identical environmental conditions (half-hourly PPFD values within $75 \mu\text{mol m}^{-2} \text{ s}^{-1}$, air temperatures within 3°C and wind speeds within 1 m s^{-1}). These requirements were frequently not met so the sample size in one year was less than for the two-tower method. Equivalent conditions were considered at time lags longer than 1 day, but as the lag between measurements increased, so did the risk of nonstationarity. Seven years (1996–2002) of data from the main tower were used for these analyses.

To explore whether and how flux uncertainty varied by environmental conditions, we binned our two-tower and successive-days flux differences by half-hourly mean wind speed, net radiation, or time of day. Basic parameters describing the distribution of these differences (i.e., mean, standard deviation, skew and kurtosis) were calculated for the various bins only when there were at least 10 differenced measurements in a given bin.

Results

The mean differences between fluxes recorded at the two Howland towers were small (Table 1). Over the entire year, for example, the mean between-tower differences for H , LE and F_{CO_2} were about 12, 23 and 5%, respectively, of the mean fluxes.

Frequency analysis indicates that the PDFs of the two-tower differences are not Gaussian (Shapiro-Wilk and Kolmogorov-Smirnov tests, $P < 0.01$). Instead, the data are strongly leptokurtic (Table 1, Figure 1), with large tails and prominent central peaks. Daytime data (characterized by greater fluxes) are

less leptokurtic than the entire data set, although the two-tower differences for all fluxes still include a number of extreme values ($> 4\sigma$). The probability of values $> 4\sigma$ in a normal distribution is ~ 0.000063 , meaning we should see such points only about once in an entire year. However, just during the summer daytime hours of 2000, differences between the towers in H , LE and F_{CO_2} exceeded 4σ on 13, 19 and 15 occasions.

We find that a double-exponential (Laplace) distribution provides a better fit to the flux errors than a normal distribution (Figure 1), capturing the strong central peak and outliers. The mean difference between the observed distributions (histograms in Figure 1) and values predicted by the double-exponential distributions across the central bins that include 90% of all observations are about half or less than those resulting from a normal distribution. For example, with a normal distribution, the mean differences between the observed and predicted frequencies across the bins encompassing 5–95% of the PDF for the summer data shown in Figure 1 are 7.5, 6.7 and 5.1% for H , LE and F_{CO_2} , respectively. The corresponding mean differences between observed frequencies and those predicted by the exponential distribution are 3.8, 3.5 and 0.7% respectively.

Table 1. Statistical properties of inferred flux uncertainties for one tower across the entire calendar year and during the growing season (days 122–295). Nighttime CO_2 fluxes were not used if $u_* < 0.25 \text{ m s}^{-1}$. Abbreviations: SD = standard deviation; H , LE and F_{CO_2} = heat, water vapor and CO_2 fluxes, respectively; JD = Julian day; R_n = net radiation (W m^{-2}); and PPF = photosynthetically active photon flux density ($\mu\text{mol m}^{-2} \text{ s}^{-1}$).

Flux	Mean difference	n	SD	Skewness	Kurtosis	$\sqrt{2}\beta$
<i>Two tower approach (2000)</i>						
H (W m^{-2})	−3.1	11,799	25.3	−1.4	23.9	19.5
JD 122–295	−4.6	5243	28.7	−1.1	11.5	23.1
$R_n > 400$	−25.0	1113	52.8	−0.4	1.3	56.9
$R_n < 100$	0.3	7830	14.6	0.8	135.4	10.4
LE (W m^{-2})	5.0	12,242	22.7	2.6	24.2	16.5
JD 122–295	9.6	5403	31.6	1.6	11.3	26.6
$R_n > 400$	15.1	1087	52.6	0.7	3.4	51.6
$R_n < 100$	1.9	8244	10.2	3.9	79.9	7.0
F_{CO_2} ($\mu\text{mol m}^{-2} \text{ s}^{-1}$)	−0.1	8688	1.9	−0.0	17.9	1.5
JD 122–295	−0.2	3659	2.7	0.0	8.2	2.5
PPFD > 1000	−0.7	1228	2.6	−0.7	6.0	2.5
Day	−0.2	6036	2.1	−0.1	15.3	1.7
Night	0.2	2652	1.2	1.5	18.0	0.9
<i>Successive days approach (1996–2002)</i>						
H (W m^{-2})	1.7	22,790	27.4	0.3	50.3	24.5
JD 122–295	1.6	12,443	27.4	0.6	16.7	24.2
$R_n > 400$	5.2	656	61.2	−0.4	1.9	67.5
$R_n < 100$	1.6	18,716	23.0	2.0	57.9	21.8
LE (W m^{-2})	−0.6	18,952	18.0	−0.8	37.7	11.3
JD 122–295	−1.0	10,591	23.0	−0.6	24.1	15.7
$R_n > 400$	−2.1	612	59.2	−0.1	2.4	60.6
$R_n < 100$	−0.3	15,497	12.2	−0.6	56.2	8.2
F_{CO_2} ($\mu\text{mol m}^{-2} \text{ s}^{-1}$)	0.1	8753	2.5	0.3	12.6	2.0
JD 122–295	0.2	4368	3.4	0.2	6.2	3.1
PPFD > 1000	0.2	930	3.9	0.3	4.7	3.8
Day	0.1	4941	2.9	0.2	10.2	2.4
Night	0.0	3812	1.9	0.7	15.3	1.5

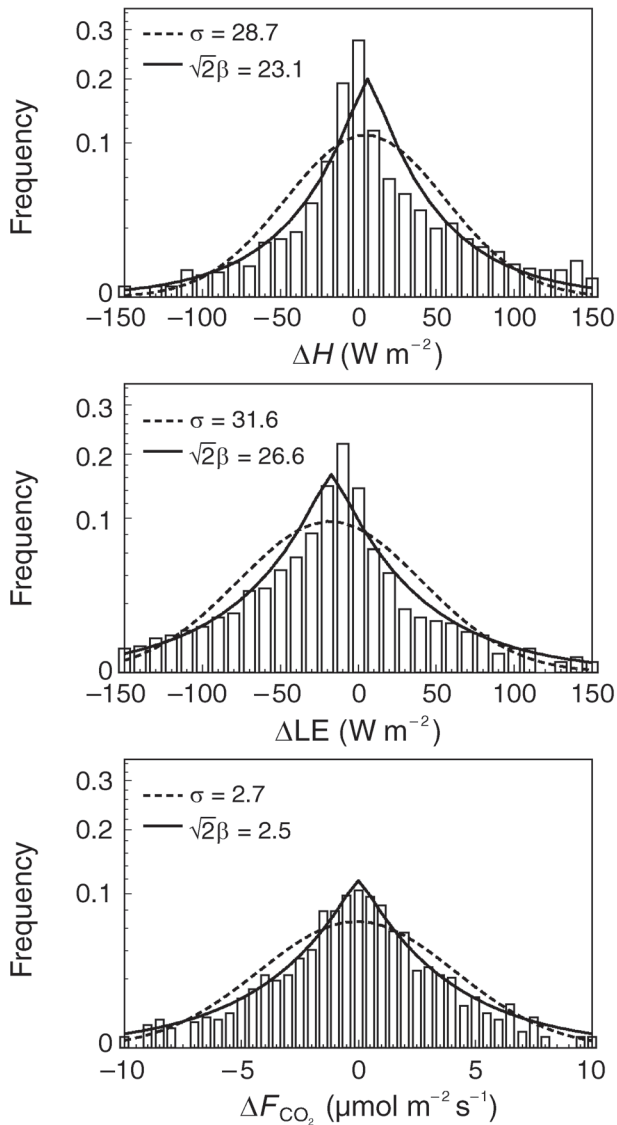


Figure 1. Flux uncertainties for H , LE and F_{CO_2} (heat, water vapor and CO_2 fluxes, respectively) are characterized by a central peak and long tails. The data better fit double exponential distributions than Gaussian distributions.

Because the uncertainty appears to follow a double exponential distribution, in the analysis that follows we use $\sqrt{2}\beta$ as our uncertainty measure because it is the double exponential equivalent of σ .

A second important result relevant to model fitting is that none of the flux uncertainties are constant (Table 1). Flux uncertainty is greater during the growing season than over the entire year and in the daytime rather than at night. Eddy flux data are heteroscedastic, with the error increasing along with the absolute magnitude of the flux (Figure 2). For H , flux uncertainty increases by a relatively constant 0.22 W m^{-2} per 1-W m^{-2} increase of flux from a minimum uncertainty of about 10 W m^{-2} . For LE , the minimum uncertainty is again around 10 W m^{-2} , but the rate of increase at -0.32 W W^{-1} is greater than for H (Figures 2A and 2B). The CO_2 flux uncertainty

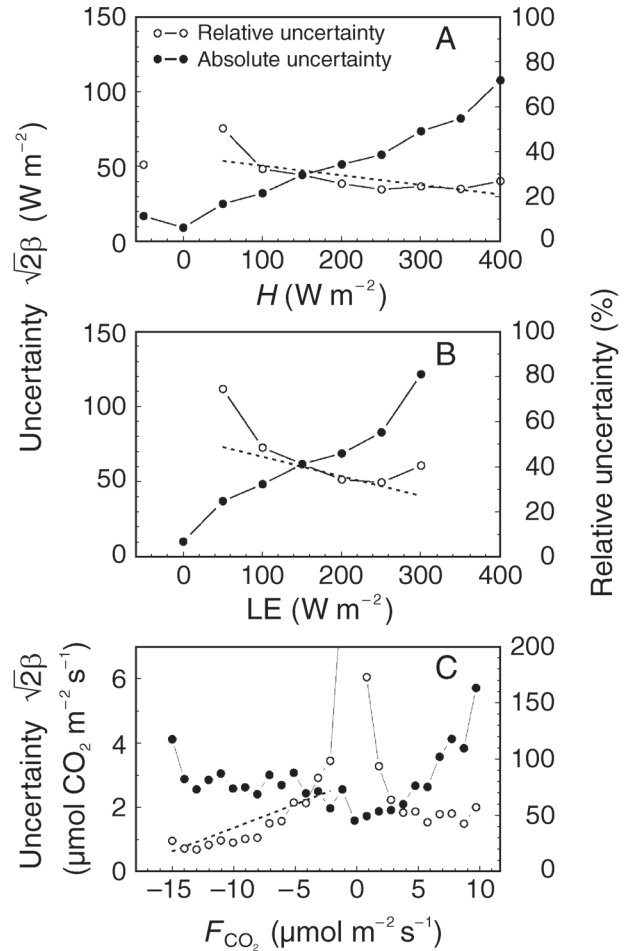


Figure 2. Absolute flux uncertainty increases as fluxes increase, but relative uncertainty decreases with increasing flux. The dashed lines show the daytime relative uncertainty estimated from turbulence statistics (Lenschow et al. 1994). Abbreviations: H , LE and F_{CO_2} = heat, water vapor and CO_2 fluxes, respectively.

(Figure 2C) appears to behave somewhat differently between night (flux > 0) and day (flux < 0). In the daytime, F_{CO_2} uncertainty increases by about $0.1 \mu\text{mol m}^{-2} \text{s}^{-1}$ per $\mu\text{mol m}^{-2} \text{s}^{-1}$ increase in uptake (negative values represent photosynthetic uptake in Figure 2C). At night, the rate of uncertainty increase with increasing exchange (respiration) is about four times greater per $\mu\text{mol m}^{-2} \text{s}^{-1}$ flux increase. Because the increase in uncertainty for all of these fluxes with an increase in flux magnitude is less than unity, the relative uncertainty ($= \sqrt{2}\beta / |F|$, where $|F|$ is the absolute value of the total flux) of the measured fluxes decreases with the absolute value of the flux. The “traditional” micrometeorological approach (Equation 16) generates approximately constant relative error during daytime (dashed lines in Figure 2) and thus also produces heteroscedastic error estimates. The similarity in relative uncertainty values generated by the Lenschow et al. (1994) method (evaluated during the daytime) and the two towers is striking.

Since solar radiation is the dominant driver of H , LE and F_{CO_2} , we examined the relationship between uncertainty and net radiation, R_n , separating out growing season from non-

growing season data. For H , there is a linear increase in uncertainty ($\sqrt{2}\beta_H$) at the rate of $0.115 \pm 0.010 \text{ W m}^{-2}$ (mean $\pm 95\%$ confidence limits, $P < 0.01$, $r^2 = 0.95$) per W m^{-2} absolute value of R_n , with a zero intercept of $4.0 \pm 3.7 \text{ W m}^{-2}$. The relationship between heat flux uncertainty and R_n is not significantly different between the growing season and non-growing season (Figure 3A). We use the absolute value of R_n in this relation because sensible heat flux to the surface increases at night as R_n becomes more negative and uncertainty is proportional to flux magnitude. Evaluating total heat flux uncertainty independently via Equation 16 yielded the same relationship with R_n as that derived from the two towers.

During the growing season, there is a similar close relationship between R_n and the uncertainty in LE measurements (Figure 3B), with $\sqrt{2}\beta_{LE}$ increasing as $0.067 \pm 0.018 \text{ W m}^{-2}$ (mean $\pm 95\%$ confidence limits, $P < 0.01$, $r^2 = 0.80$) per $\text{W m}^{-2} R_n$.

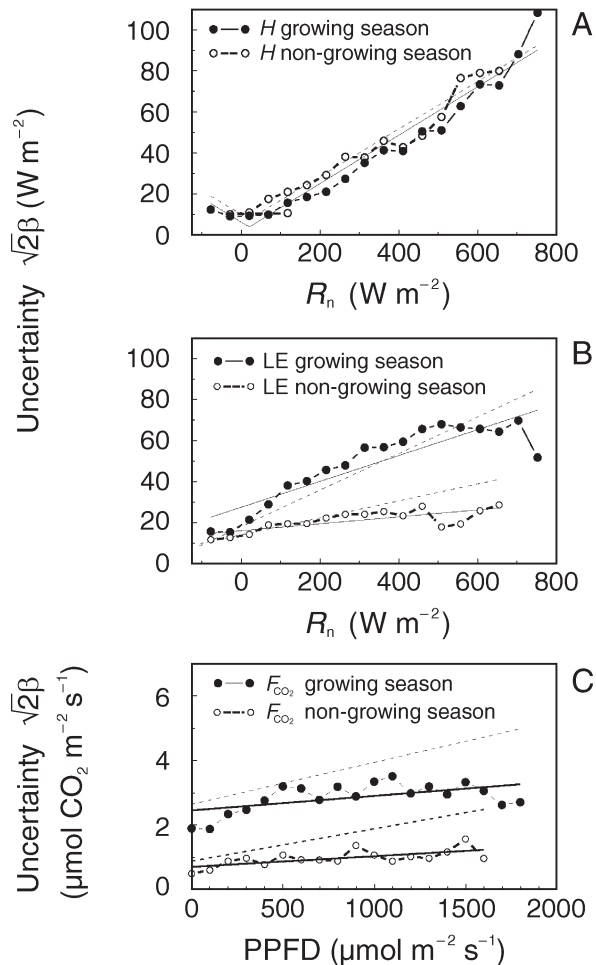


Figure 3. Flux uncertainty for H and LE is tightly correlated with net radiation, whereas F_{CO_2} uncertainty is only weakly correlated with solar radiation. For H uncertainty, the relationship between R_n and uncertainty is the same during the growing season and non-growing season. Dashed lines show daytime uncertainty calculated by the Lenschow et al. (1994) method. For H and LE uncertainty there is good agreement with the two-tower approach. Abbreviations: H , LE and F_{CO_2} = heat, water vapor and CO_2 fluxes, respectively; and R_n = net radiation.

The zero intercept of this relationship is $21.5 \pm 7.4 \text{ W m}^{-2}$. During the non-growing season at the Howland forest, stomatal closure and frozen soils limit LE flux (Hollinger et al. 1999) and also, apparently, LE uncertainty (Figure 3B). Non-growing season LE uncertainty increases as a function of R_n at only about one third the growing season rate ($\sqrt{2}\beta_{LE} = 0.018 \pm 0.009 R_n + 8.0 \pm 3.1$, $P < 0.01$, $r^2 = 0.58$). The Lenschow et al. (1994) model again provided a good approximation of uncertainty during daytime conditions.

The growing-season and non-growing season uncertainty in F_{CO_2} provides an interesting contrast to that of H and LE in that $\sqrt{2}\beta_{\text{CO}_2}$ is only weakly related to solar forcing (Figure 3C). Although the relations between PPFD and F_{CO_2} uncertainty are significant, they account for well under half of the observed variation in $\sqrt{2}\beta_{\text{CO}_2}$ (growing season $\sqrt{2}\beta_{\text{CO}_2} = 0.00045 \pm 0.00035 \text{ PPFD} + 2.45 \pm 0.37$, $P < 0.05$, $r^2 = 0.30$, non-growing season $\sqrt{2}\beta_{\text{CO}_2} = 0.00033 \pm 0.00020 \text{ PPFD} + 0.70 \pm 0.19$, $P < 0.05$, $r^2 = 0.44$). The slopes of the growing-season and non-growing-season relationships are not significantly different but the growing-season intercept is about three times larger than the non-growing-season intercept. Our implementation of the Lenschow et al. model (1994) over-estimated uncertainty compared to the two-tower approach and this difference increased with increasing PPFD (Figure 3C).

For F_{CO_2} , uncertainty is also related to wind speed (\bar{u}) (Figure 4), with uncertainty decreasing as wind speed increases. The slope and zero intercepts in the wind/uncertainty relationships were significantly different between the growing season and non-growing season (growing season $\sqrt{2}\beta_{\text{CO}_2} = 3.76 \pm 0.74 - 0.43 \pm 0.21 \bar{u}$, $P < 0.01$, $r^2 = 0.85$, non-growing season $\sqrt{2}\beta_{\text{CO}_2} = 0.86 \pm 0.17 - 0.056 \pm 0.046 \bar{u}$, $P < 0.05$, $r^2 = 0.66$). However, neither the slopes nor intercepts in the wind-uncertainty relationships were significantly different between growing season daytime and nocturnal data (Figure 4B). For daytime conditions, uncertainty calculated by Equation 16 similarly decreases with increasing wind speed (Figure 4B), but values are about $1 \mu\text{mol m}^{-2} \text{ s}^{-1}$ larger (+25 to 80%) than the two-tower estimates.

Successive days approach

The successive days approach to estimating $\sqrt{2}\beta$ yielded relationships with wind speed (for F_{CO_2}) and net radiation (for H and LE) that were similar to and consistent with those derived using the two-tower approach (Figure 5). However, the successive days approach generally resulted in estimates of flux uncertainty that were higher than those obtained by the two-tower method. Presumably this is because, besides the measurement uncertainty, there is additional variability in each pair of measured fluxes because the measurements were conducted a full 24 h apart under similar but not identical environmental conditions. We found that the slopes of the wind- F_{CO_2} uncertainty relationships calculated by the two-tower and successive days approaches were not significantly different ($P = 0.10$) but that the zero intercepts were significantly different ($P < 0.05$). The zero intercept obtained via the successive days approach was about $1.4 \mu\text{mol m}^{-2} \text{ s}^{-1}$ (36%) higher than obtained with data from both towers. For H and LE, we found that the successive-days approach overestimated the zero in-

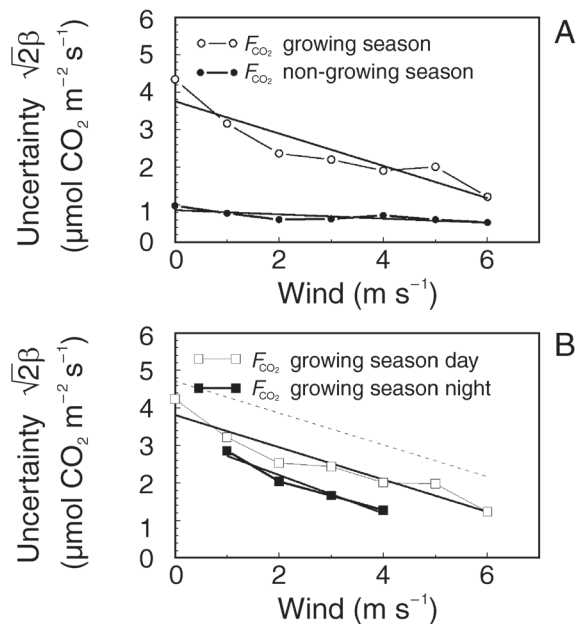


Figure 4. Carbon dioxide flux (F_{CO_2}) uncertainty decreases as wind speed increases. The relationship is different between growing season and non-growing season, but within a season, it is similar between night and day. The dashed line shows the daytime uncertainty calculated after Lenschow et al. (1994).

tercept in the relationships between uncertainty and R_n relative to the two-tower approach (probability H intercepts are equal = 0.0002 and probability LE intercepts are equal = 0.0514) but yielded similar slopes (probability H slopes are equal = 0.185 and probability LE slopes are equal = 0.635).

Support for the idea that nonstationarity contributes additional uncertainty to our F_{CO_2} uncertainty estimates comes from an analysis of the uncertainty that results from extending the paired data comparison beyond 1 day. For example, using daytime (PPFD > 5 $\mu\text{mol m}^{-2} \text{ s}^{-1}$) mid-growing season (JD 152–273) CO_2 fluxes, we found that uncertainty was positively correlated ($r = 0.90$, $P = 0.001$) with the length of the time period between successive samples, and increased at a rate of about 1% per day of lag. However, for both H and LE, σ was uncorrelated with the length of the lag time ($r = -0.24$, $P = 0.13$, and $r = 0.21$, $P = 0.20$, respectively). Figure 3B, however, suggests that a similar analysis for LE that extended between growing and non-growing season would show similar evidence of nonstationarity.

The successive days method indicated that the flux uncertainty follows an approximately exponential distribution (results not shown), at least for H and F_{CO_2} . However, the LE distribution has a tighter central peak and fatter tails, than even an exponential distribution.

Overall, the statistical properties of the flux deviations were similar for the two-tower and successive day approaches (Table 1). The persistent mean difference in H and LE (-25 and 15 W m^{-2} , respectively, for $R_n > 400$) for the two-tower approach may reflect systematic differences in the tower footprints (Hollinger et al. 2004); these differences were much smaller (5.2 and -2.1) for the successive days method.

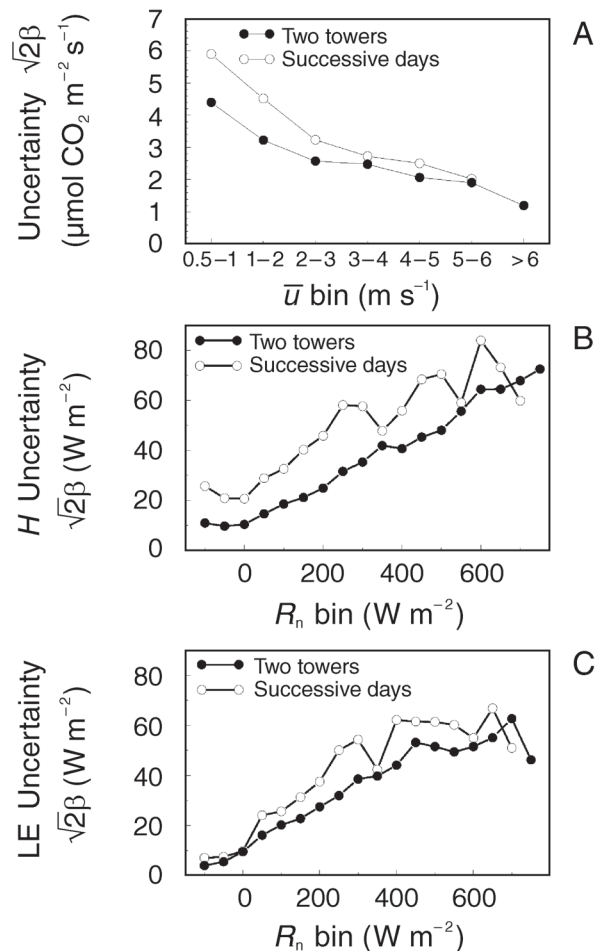


Figure 5. Uncertainties estimated by the successive days approach are similar to, but generally higher than, estimates resulting from the two-tower method. Abbreviations: H and LE = heat and water vapor fluxes, respectively; R_n = net radiation; and \bar{u} = wind speed.

Using uncertainty estimates in model parameter estimation

The preceding analysis of uncertainty provides the information needed to carry out an ML estimation of model parameters from flux data; specifically information on the measurement uncertainty, σ , and the appropriate PDF. Without this information, such analyses lack rigor and may lead to incorrect conclusions about the most likely parameter values. Our results, however, indicate that there are several ways of specifying uncertainty and that more than one PDF may sometimes be suitable. The specific choice of these characteristics and the related issue of how noise is added back into Monte Carlo simulations have a direct impact on both the parameter estimates and their uncertainty.

Maximum likelihood analysis and Monte Carlo simulation based on uncertainty data from our two-tower approach indicate that for the simple “big-leaf” model of Equation 6, there is a region of equifinality where there are many parameter sets which have an almost equal likelihood, given the observed flux data and its uncertainty (Figure 6). The different weighting (likelihood functions) associated with Gaussian or double exponential PDFs generate different likely parameter sets. In

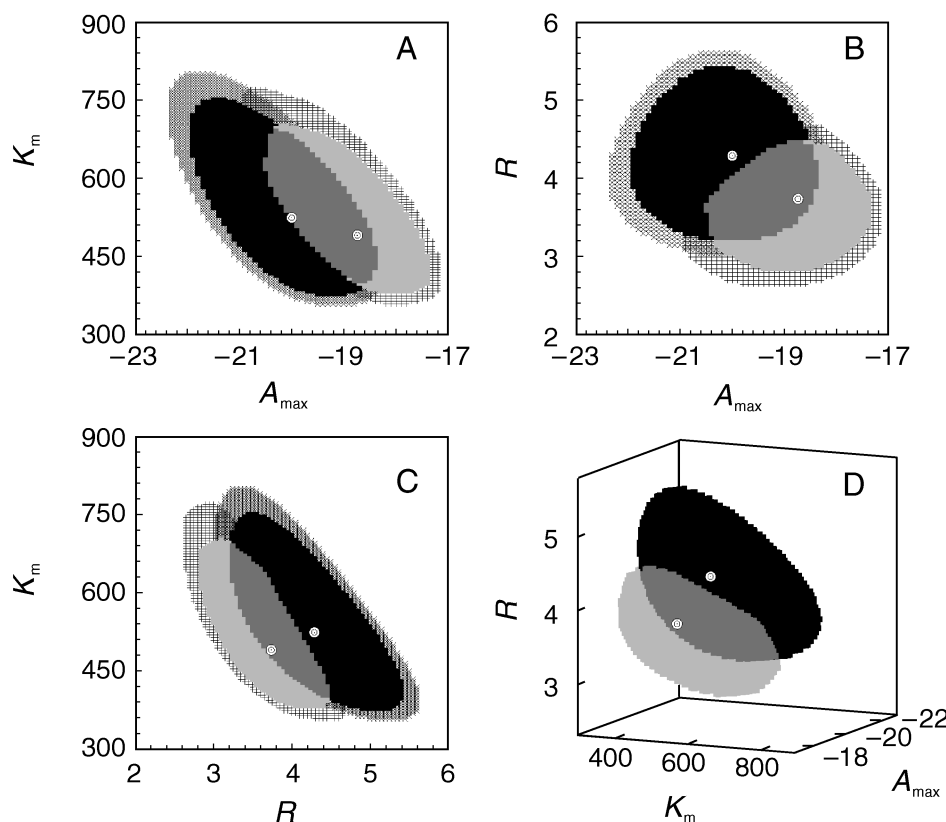


Figure 6. Parameter estimates for a Michaelis-Menten model of leaf photosynthesis ($= A_{\max}/(K_m + I) + R$) determined from June 2000 carbon dioxide (CO_2) flux data. The black region represents the 95% uncertainty limits of parameter triplets assuming Gaussian uncertainties with $\sigma = 2.7 \mu\text{mol m}^{-2} \text{s}^{-1}$, and the gray indicates the corresponding 95% uncertainty region assuming the double exponential probability density function with $\sqrt{2}\beta = 2.5 \mu\text{mol m}^{-2} \text{s}^{-1}$. The cross-hatched areas indicate the 99% uncertainty regions. The first three panels (A–C) represent different 2-D projections of the parameter sets and the final panel (D) shows a 3-D representation. Abbreviations: A_{\max} = maximum rate of uptake; K_m = half-saturation constant; I = incident PPFD; and R = ecosystem respiration. Units for A_{\max} and R are $\mu\text{mol CO}_2 \text{m}^{-2} \text{s}^{-1}$, and for K_m are $\mu\text{mol PPFD m}^{-2} \text{s}^{-1}$.

both cases, the variation of individual pairs of parameters among sets are highly correlated (Table 2). Principal components analysis of the model parameters highlights this correlation: for the exponential error distribution, for example, the first two components accounted for 63 and 36% of the total variance, respectively, whereas the third component accounted for less than 1% of the total variance. The model has three dimensions, but the correlation of the parameters essentially reduces this to just two. More complex models likely have even greater degrees of redundancy.

Because the parameters are correlated, one must consider the joint distribution of parameters instead of comparing or testing a single parameter value. The appropriate criterion is the chi-squared statistic (Equations 13 or 14, depending on PDF). Critical values for the parameter values can be generated by ranking the parameter sets resulting from the Monte Carlo simulations by their χ^2 value, and selecting χ^2 values corresponding to the appropriate percentile. Chi-square values can also be used to evaluate the fit of different models to the same data.

Using this criterion, the parameter estimates derived from assuming Gaussian or exponential error distributions are different; at least, the least squares optimum is greater than the 95-percentile χ^2 value of the exponential distribution, although the converse is not true. The uncertainty in the original measurements is critical here: larger uncertainty in the measurements means larger uncertainty in the parameter estimates, which in turn means a larger 95% χ^2 value and a decreased ability to detect significant differences.

The big-leaf model of Equation 6 has useful predictive properties but is physiologically incorrect. The Norman model (Equations 7–12) scales leaf-level photosynthesis directly to

Table 2. Summary of model parameters derived from Monte Carlo simulations ($n = 4000$). June 2000, main tower data only. Abbreviations: A_{\max} = maximum rate of uptake ($\mu\text{mol m}^{-2} \text{s}^{-1}$); K_m = half-saturation constant ($\mu\text{mol photons m}^{-2} \text{s}^{-1}$); and R = ecosystem respiration ($\mu\text{mol m}^{-2} \text{s}^{-1}$).

	A_{\max}	K_m	R
<i>Descriptive statistics</i>			
Normal distribution, minimizing least squares ($\chi^2 = \Sigma(\epsilon^2)$)			
Optimum	-20.0	524.8	4.3
Mean \pm 1 SD	-20.1 \pm 0.6	529 \pm 68	4.3 \pm 0.4
Exponential distribution, minimizing absolute value ($\chi^2 = \Sigma \text{abs}(\epsilon)$)			
Optimum	-18.7	491.2	3.7
Mean \pm 1 SD	-18.8 \pm 0.4	493 \pm 50	3.7 \pm 0.3
<i>Pairwise correlations</i>			
Normal distribution			
A_{\max}		-0.63	-0.01
K_m	-0.63		-0.73
R_d	-0.01	-0.73	
Exponential distribution			
A_{\max}		-0.56	-0.09
K_m	-0.56		-0.74
R_d	-0.09	-0.74	

the canopy and can be solved with the simulated annealing technique to yield leaf-level physiological parameters. Because NEE in this model is the product of a physiological capacity and LAI, leaf-level physiological parameters are unconstrained by the data (e.g., high A_{leaf} and low LAI fit the data as do low A_{leaf} and high leaf area index; Figure 7A). The model can be constrained by specifying the LAI, and at a value of about 5.5, the most likely leaf-level parameter values inferred from flux data are superficially similar to literature values (calculated from Alexander et al. 1995) determined via a photosynthesis cuvette (Table 3). Independent estimates suggest that Howland LAI is in the range of 5–7.

Comparing the χ^2 values for the big-leaf and sun-shade models indicates only a slight improvement in fit results from the more “correct” sun-shade model and that the fit slightly improves with increasing LAI. The χ^2 values that result from using literature values of leaf-level parameters rather than ML estimates from flux data indicate a considerably poorer fit to the data (Table 3). An estimate of the uncertainty in the cuvette

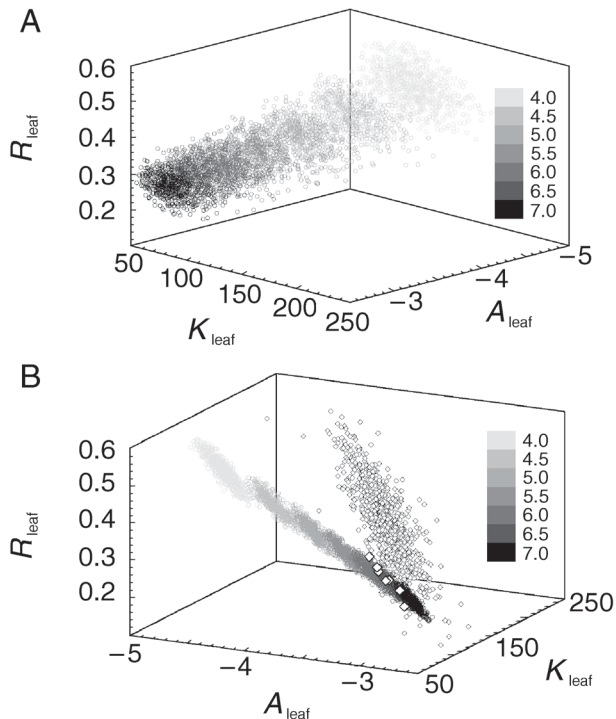


Figure 7. Parameter estimates for a Michaelis-Menten model of leaf photosynthesis ($= A_{\text{leaf}}I/(K_{\text{leaf}} + I) + R_{\text{leaf}}$) embedded within the sun-shade model of Norman (1982) (all units are $\mu\text{mol m}^{-2} \text{s}^{-1}$). (A) The darkness of the points represents the fixed model leaf area index (LAI). Leaf photosynthetic parameters that fit the data decrease in magnitude as canopy LAI increases. (B) The same data as above rotated to the right by $\sim 120^\circ$ and with maximum likelihood estimates of leaf level parameters (small diamonds) obtained from cuvette data in Alexander et al. (1995) using an uncertainty of $\sqrt{2}\beta = 0.1 \mu\text{mol m}^{-2} \text{s}^{-1}$. The parameter values derived from leaf-level data intersect those determined from tower-level NEE and the sun-shade model at a LAI of 6–6.5 (large diamonds). Abbreviations: A_{leaf} = maximum rate of leaf photosynthesis ($\mu\text{mol CO}_2 \text{ m}^{-2} \text{ s}^{-1}$); K_{leaf} = half-saturation constant ($\mu\text{mol photons m}^{-2} \text{ s}^{-1}$); I = incident PPFD; and R_{leaf} = leaf respiration ($\mu\text{mol CO}_2 \text{ m}^{-2} \text{ s}^{-1}$).

Table 3. Maximum likelihood parameter estimates of Michaelis-Menten model parameters based on big-leaf and sun-shade model formulations. Abbreviations: LAI = leaf area index; A_{leaf} = maximum rate of leaf photosynthesis ($\mu\text{mol CO}_2 \text{ m}^{-2} \text{ s}^{-1}$); K_{leaf} = half-saturation constant ($\mu\text{mol photons m}^{-2} \text{ s}^{-1}$); R_{leaf} = leaf respiration ($\mu\text{mol CO}_2 \text{ m}^{-2} \text{ s}^{-1}$); and 99-% = 99th percentile.

LAI	A_{leaf}	K_{leaf}	R_{leaf}	χ^2
Big-leaf	-18.80	495.9	3.734	1.21343
4.0	-4.69	131.4	0.467	1.21165
4.5	-4.17	117.3	0.415	1.21132
5.0	-3.75	105.0	0.374	1.21117
5.5	-3.41	94.4	0.340	1.21099
6.0	-3.12	85.1	0.311	1.21084
6.5	-2.88	76.9	0.287	1.21077
7.0	-2.67	69.6	0.267	1.21065
Leaf cuvette data	-3.45	157.2	0.350	1.37119
99-% leaf data (LAI = 6)	-2.94	76.0	0.304	1.21448

data would be useful here, and although Alexander et al. (1995) do not report such, it would probably be small. We assume for Figure 7B that the measurement uncertainty of the cuvette data ($\sqrt{2}\beta$) = $0.1 \mu\text{mol m}^{-2} \text{ s}^{-1}$, and plot the resulting Monte Carlo estimates of leaf-level parameter sets derived from leaf-level data on the same figure as those derived from eddy flux data and the sun-shade model. The χ^2 values of the leaf-level parameter estimates determined from cuvette data intersect those determined from flux data in the LAI = 6–6.5 region, a value consistent with independent estimates of LAI.

The models are compared to NEE from flux data $\pm 95\%$ uncertainty limits, where $\sqrt{2}\beta$ is based on \bar{u} in Figure 8. The big-leaf and sun-shade models (when they use leaf-level parameters determined by ML from the flux data) yield virtually identical results (symbols overlap). Not surprisingly, the sun-

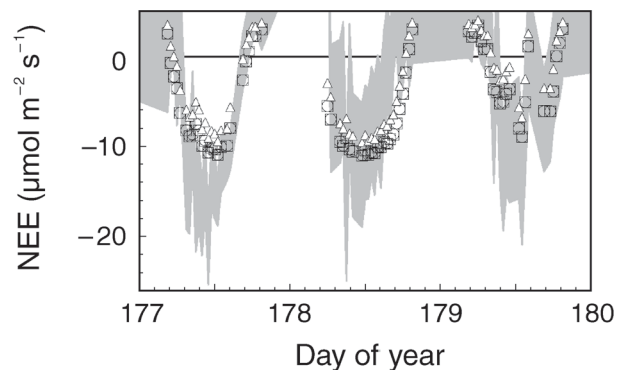


Figure 8. Comparison of modeled and measured net ecosystem exchange (NEE). Symbols: \square = the big-leaf model; \circ = sun-shade model at a leaf area index (LAI) of 6; and \triangle = the sun-shade model (LAI = 6) when the photosynthetic parameters come from leaf-level measurements. The 95% NEE uncertainty limits are indicated by the vertical width of the shaded area.

shade model using literature-derived leaf parameters fits the flux data less well (76% of the modeled values lie within the 95% uncertainty level of the data whereas 81% of the big-leaf and sun–shade model results lie within the 95% band).

Discussion

Flux data are characterized by peaked (non-normal) error distributions. These distributions apparently result from several factors. First, for all fluxes, the data are heteroscedastic, with the error increasing along with the absolute magnitude of the flux. When this heteroscedasticity is combined with the frequency of different flux magnitudes (far more instances of low than high values), the result is a strongly peaked error distribution. For example, LE is zero at night and during the winter months; over the course of a year about 2/3 of all LE values are recorded from these time periods. A second factor leading to the non-normal error distribution relates to real world problems with measurement systems (Press et al. 1993). Occasionally, “glitches” caused by power fluctuations, insects in the path of a sonic anemometer, contamination, or other factors, result in measured values that are far from correct. Flux data are characterized by extreme outliers, despite the best efforts of researchers. If it is assumed that the error is normally distributed with constant variance, then the best-fit parameters of a model (those with the maximum likelihood of accounting for the observed data) are determined by minimizing the sum of the squares of the deviations between the model and the data points. Because the deviations are squared, extreme outliers that have no biological significance can exert an enormous effect on the model parameters.

The double exponential distribution, in addition to better describing real flux data, has the advantage that the maximum likelihood estimator is calculated by minimizing the mean absolute deviation, considerably reducing the impact of outliers. Press et al. (1993) discuss additional error distributions in which weights of the points first increase with deviation and then decrease, minimizing the impact of the most deviant points in the estimation of parameters.

For all of the fluxes, uncertainty increases with flux magnitude. This is unlikely to be a property of the measurement system (sonic anemometer, gas analyzer, etc.) and is thus apparently a property of the intermittency of turbulent transport. The length scale of the dominant eddies responsible for most turbulent transport over a forest is relatively large (Raupach et al. 1996) and there are few of these in a half-hour integration period. This sort of quasi-Poisson behavior (most of the flux carried in a few events) would manifest itself in the observed heteroscedasticity.

The excellent agreement between sensible and latent heat flux uncertainties calculated by the two-tower and traditional (Lenschow et al. 1994) approaches is heartening and suggests that the assumptions of cospectral shape and integral timescale are reasonable. The close agreement also implies that the majority of the total uncertainty, measured by the two-tower approach, is accounted for by the turbulent uncertainty, rather than measurement system or footprint uncertainty. Support for this conclusion comes from an AmeriFlux calibration visit to

Howland that found CO₂ flux measurement system uncertainty to be only 0.8 μmol m⁻² s⁻¹ (R. Evans, USDA Forest Service, Durham, NH, unpublished data).

Contrary to results for *H* and LE, the Lenschow et al. (1994) approach overestimated *F*_{CO₂} uncertainty, suggesting our integral timescale estimate is too large or problems with the cospectral shape model. The difference in the behavior of *F*_{CO₂} uncertainty from that of *H* and LE with wind speed may result from differences within the forest in the location of the exchange sites. For *H* and LE, most of the plant–atmosphere exchange occurs at the top of the canopy, and the exchange is generally of the same sign from the top of the canopy to the forest floor (out-going during the daytime). For daytime CO₂ exchange, however, uptake occurs at the top of the canopy while the forest floor is a strong source of CO₂. We speculate that intermittent penetration of turbulent eddies through the canopy at low wind speeds leads to less efficient mixing of forest floor and canopy air than at higher wind speeds and thus greater variability (higher uncertainty) of CO₂ fluxes recorded at low wind speed. Another way to express this idea is that there may be different cospectral shapes for top-of-canopy and below-canopy exchange. Evaluation of CO₂ flux uncertainty over other canopy types (short crops or grassland) would address this hypothesis.

One important additional consequence of our analysis is that the uncertainty of data recorded by an open-path CO₂ analyzer is likely to be larger than that using a closed-path system. This is because calculation of *F*_{CO₂} with the former requires information on *H* and LE. Thus the uncertainties inherent in the measurements of *H* and LE will contribute to the final uncertainty of *F*_{CO₂}.

We evaluated big-leaf and sun–shade canopy models using the ML and Monte Carlo techniques as an example of the application of uncertainty data. These examples illustrate several important points including equifinality of parameter sets, impact of PDF, lack of independence of model parameters and the non-constraint of a model by flux data. Although a detailed analysis of the models was not the goal here, we observe that whereas incorporating a simple canopy model only trivially reduced the mean absolute error, it introduced a framework that allowed scaling from leaf-level data. Leaf-level data could then provide a constraint on the LAI of the canopy model; bottom-up (leaf-level) and top-down (eddy flux) parameters only intersected over a narrow range of LAI values that were, in fact, consistent with independent LAI measurements at the site.

The NEE calculated via the models was frequently (about 20% of the time) outside of the 95% confidence bands of the flux data (e.g., Figure 8). This strongly suggests that further improvements of the models are possible. Given that these models are insensitive to temperature or vapor pressure deficit, there are obvious starting points for improvement.

Flux data are not truth—instead they represent “correct” values plus or minus some amount of measurement error, which we here call uncertainty. Traditional approaches appear to work well in characterizing uncertainty in *H* and LE. Uncertainty in flux data can also be estimated by comparing results from two towers measuring similar vegetation in slightly dif-

ferent places at the same time or by comparing results from the same tower under similar conditions at different times. Both analyses indicate that the uncertainty in Howland flux data, and by analogy, probably all flux sites, is better characterized by a double-exponential distribution than by a normal distribution. This has the consequence that parameter values of models of surface-atmosphere exchange determined from the data should not use ordinary least squares minimization but instead should seek to minimize the sum of the absolute deviations between model outputs and data. Before this conclusion is widely adopted, however, it should be examined critically at other sites because minimizing based on the absolute deviation may result in a different bias than OLS, and bias is critical to annual sums of flux data (A.D. Richardson and D.Y. Hollinger, unpublished results).

A second result is that the uncertainty in flux data is not a constant. The uncertainty for all fluxes increases with increasing magnitude of the flux. More usefully, for H and LE during the growing season, uncertainty increases roughly as $0.1R_n$ and $0.08R_n$ above a base uncertainty ($R_n = 0$) of $\sim 10 \text{ W m}^{-2}$. There is no seasonality in the uncertainty of H at the evergreen Howland forest, indicating that uncertainty for this flux is not modulated by biology, but is instead controlled purely by physical factors. The uncertainty of LE , however, responds to R_n differently in the growing and non-growing season, suggesting a biological cause. We would expect that uncertainty in H and LE in a deciduous forest to behave differently depending upon presence or absence of the canopy.

For CO_2 flux, we found that flux uncertainty correlated with wind velocity, decreasing roughly by half as mean wind speed increases from $\sim 1\text{--}4 \text{ m s}^{-1}$. We hypothesize that intermittency of atmospheric mixing in the two-level structure of a forest, especially in the daytime when the canopy is a sink and the soil is a source for CO_2 , adds to the uncertainty of forest-atmosphere CO_2 fluxes. Enhanced mixing at higher wind speeds would reduce this uncertainty. A test of this idea would be to determine whether CO_2 flux uncertainty remains a function of wind speed in a structurally more simple system such as a grassland, crop, or deciduous forest after leaf fall. A consequence of the relationship between CO_2 flux uncertainty and wind speed is that models of flux exchange may be better constrained at windy sites and structurally simple sites than at less windy or structurally complex sites.

Uncertainty estimated by the successive days approach is generally greater than that estimated by two towers. One reason for this result may be that nocturnal events such as rainfall or frost change the state of the ecosystem between measurements. The successive days estimates of flux measurement uncertainty should be adjusted to counter this additional uncertainty that is not part of the real (instantaneous) flux measurement uncertainty. We therefore recommend decreasing successive days estimates of H by a constant 20 W m^{-2} and for F_{CO_2} and LE , reducing σ calculated using successive days to about 75–80% of the estimated value.

Uncertainty information is a critical part of parameter estimation with the Maximum Likelihood technique and necessary for estimating parameter confidence regions. Flux uncertainty information is also necessary for evaluating independ-

ently formulated models against flux data, when using more sophisticated forecasting techniques such as the Kalman filter (Jarvis et al. 2004), and in other data-model fusion approaches.

Acknowledgments

D.H. wishes to thank A. Mäkelä and H. Hasenauer for their organization of the excellent 2004 IUFRO conference on Modeling Forest Production. Many of the ideas in this paper were stimulated by participation at this conference. We thank the International Paper Company, Ltd. for providing access to the research site in Howland, Maine. The Howland flux research was supported by the USDA Forest Service Northern Global Change Program, and the Office of Science (BER), U.S. Department of Energy, through Interagency Agreement No. DE-AI02-00ER63028 and through the Northeast Regional Center of the National Institute for Global Environmental Change under Cooperative Agreement No. DE-FC03-90ER61010. The Howland Forest multi-year CO_2 flux and climate data set is available at <http://public.ornl.gov/ameriflux/Data/index.cfm> subject to AmeriFlux "Fair-use" rules.

References

- Alexander, J.D., J.R. Donnelly and J.B. Shane. 1995. Photosynthetic and transpirational responses of red spruce understory trees to light and temperature. *Tree Physiol.* 15:393–398.
- Baldocchi, D.D. 2003. Assessing the eddy covariance technique for evaluating carbon dioxide exchange rates of ecosystems: past, present and future. *Global Change Biol.* 9:479–492.
- Bevington, P.R. and D.K. Robinson. 1992. Data reduction and error analysis for the physical sciences. McGraw Hill, New York, 328 p.
- Businger, J.A. 1986. Evaluation of the accuracy with which dry deposition can be measured with current micrometeorological techniques. *J. Clim. Appl. Meteorol.* 25:1100–1124.
- Davidson, E.A., A.D. Richardson, K.E. Savage and D.Y. Hollinger. 2005. A distinct seasonal pattern of the ratio of soil respiration to total ecosystem respiration in a spruce-dominated forest. *Global Change Biol.* In press.
- Fernandez, I.J., L.E. Rustad and G.B. Lawrence. 1993. Estimating total soil mass, nutrient content and trace metals in soils under a low elevation spruce-fir forest. *Can. J. Soil Sci.* 73:317–328.
- Finkelstein, P.L. and P.F. Sims. 2001. Sampling error in eddy correlation flux measurements. *J. Geophys. Res.* 106(D4):3503–3509.
- Franks, S.W., K.J. Beven, P.F. Quinn and I.R. Wright. 1997. On the sensitivity of soil-vegetation-atmosphere transfer SVAT schemes: equifinality and the problem of robust calibration. *Agric. For. Meteorol.* 86:63–75.
- Goulden, M.L., J.W. Munger, S.-M. Fan, B.C. Daube and S.C. Wofsy. 1996. Measurements of carbon sequestration by long-term eddy covariance: methods and a critical evaluation of accuracy. *Global Change Biol.* 2:169–182.
- Hollinger, D.Y., F.M. Kelliher, E.-D. Schulze et al. 1995. Initial assessment of multi-scale measures of CO_2 and H_2O flux in the Siberian taiga. *J. Biogeogr.* 22:425–431.
- Hollinger, D.Y., S.M. Goltz, E.A. Davidson, J.T. Lee, K. Tu and H.T. Valentine. 1999. Seasonal patterns and environmental control of carbon dioxide and water vapor exchange in an ecotonal boreal forest. *Global Change Biol.* 5:891–902.
- Hollinger, D.Y., J. Aber, B. Dail et al. 2004. Spatial and temporal variability in forest-atmosphere CO_2 exchange. *Global Change Biol.* 10:1689–1706.
- Horst, T.W. 1997. A simple formula for attenuation of eddy fluxes measured with first-order-response scalar sensors. *Boundary-Layer Meteorol.* 82:219–233.

- Horst, T.W. 2000. On frequency response corrections for eddy covariance flux measurements. *Boundary-Layer Meteorol.* 94:517–520.
- Jarvis, A.J., V.J. Stauch, K. Schulz and P.C. Young. 2004. The seasonal temperature dependency of photosynthesis and respiration in two deciduous forests. *Global Change Biol.* 10:939–950.
- Lenschow, D.H., J. Mann and L. Kristensen. 1994. How long is long enough when measuring fluxes and other turbulent statistics? *J. Atmos. Oceanic Technol.* 11:661–673.
- Mahrt, L. 1998. Flux sampling errors from aircraft and towers. *J. Atmos. Oceanic Technol.* 15:416–429.
- Mann J. and D.H. Lenschow. 1994. Errors in airborne flux measurements. *J. Geophys. Res.* 99(D7):14,519–14,526.
- Massman, W.J. 2000. A simple method for estimating frequency response corrections for eddy covariance systems. *Agric. For. Meteorol.* 104:185–198.
- Massman, W.J. 2001. Reply to comment by Rannik on “A simple method for estimating frequency response corrections for eddy covariance systems.” *Agric. For. Meteorol.* 107:247–251.
- Massman, W.J. and X. Lee. 2002. Eddy covariance flux corrections and uncertainties in long term studies of carbon and energy. *Agric. For. Meteorol.* 113:121–144.
- Metropolis, N., A.W. Rosenbluth, M.N. Rosenbluth, A.H. Teller and E. Teller. 1953. Equation of state calculations by fast computing machines. *J. Chem. Phys.* 21:1087–1092.
- Moncrieff, J.B., Y. Malhi and R. Leuning. 1996. The propagation of errors in long-term measurements of land-atmosphere fluxes of carbon and water. *Global Change Biol.* 2:231–240.
- Morgenstern, K., T.A. Black, E.R. Humphreys et al. 2004. Sensitivity and uncertainty of the carbon balance of a Pacific Northwest Douglas-fir forest during an El Niño/La Niña cycle. *Agric. For. Meteorol.* 123:201–219.
- Norman, J.M. 1980. Interfacing leaf and canopy light interception models. *In Predicting Photosynthesis for Ecosystem Models.* Eds. J.D. Hesketh and J.W. Jones. CRC Press, Boca Raton, FL, pp 49–67.
- Norman, J.M. 1982. Simulation of microclimates. *In Biometeorology in Integrated Pest Management.* Eds. J.L. Hatfield and I.J. Thomason. Academic Press, New York, pp 65–99.
- Press, W.H., S.A. Teukolsky, W.T. Vetterling and B.P. Flannery. 1993. *Numerical recipes in Fortran 77: the art of scientific computing.* Cambridge University Press, New York, 992 p.
- Raupach, M.R., J.J. Finnigan and Y. Brunet. 1996. Coherent eddies and turbulence in vegetation canopies: the mixing-layer analogy. *Boundary-Layer Meteorol.* 78:351–382.
- Ross, J. 1981. *The radiation regime and architecture of plant stands.* Dr. W. Junk, The Hague, 391 p.
- Schulz, K., A. Jarvis and K. Beven. 2001. The predictive uncertainty of land surface fluxes in response to increasing ambient carbon dioxide. *J. Climate* 14:2551–2562.
- Taylor, J.R. 1997. *An introduction to error analysis.* University Science Books, Sausalito, CA, 327 p.
- Twine, T.E., W.P. Kustas, J.M. Norman et al. 2000. Correcting eddy-covariance flux estimates over a grassland. *Agric. For. Meteorol.* 103:279–300.
- Van Wijk, M.T. and W. Bouten. 2002. Simulating daily and half-hourly fluxes of forest carbon dioxide and water vapor exchange with a simple model of light and water use. *Ecosystems* 5:597–610.